◇ Infinite Science | Publishing

Non-destructive defect detection of LPBF-manufactured A205 aluminium alloy lattice structures

B. B. Çelik[1*], E. Beevers[1], and B. Van Hooreweder[1]

[1] Department of Mechanical Engineering, KU Leuven, Leuven, Belgium
[*] Corresponding author, email: berkbaris.celik@kuleuven.be

Abstract

Engineering and design have been altered significantly by the use of metal lattice structures. Laser Powder Bed Fusion (LPBF) enables the manufacturing of such complex three-dimensional structures with a degree of complexity and accuracy that is impossible by conventional manufacturing. However, LPBF can cause defects, e.g. small internal porosities. For part qualification, defects are ideally observed by a non-destructive inspection. Therefore, this study explores the capabilities of the impulse excitation technique to detect defects in LPBF bulk and lattice parts. Samples in the high-strength aluminium alloy A205 with and without selectively induced defects are investigated. Measurements indicated the successful detection of selectively placed internal defects based on different resonant frequencies of defect-free and defective samples.

Keywords: Laser Powder Bed Fusion, lattice structures, defect detection, impulse excitation technique

1. Introduction

Production of complex-shaped cellular structures has been made possible by the exponential growth of additive manufacturing (AM) techniques. LPBF offers a desirable option to produce complex near-net-shape geometries while consuming minimum material compared to other AM processes. The LPBF method facilitates manufacturing metal lattice structures (MLS) because of its nearly infinite design freedom [1]. Typically, lattices are highly porous structures, meaning they have an open form consisting of a large volume of pores in the solid material. Lattice structures are divided into open-cell and closed-cell varieties. An open-cell lattice structure is a porous network with interconnecting pores [2]. The unit cells in a closed-cell lattice structure, are isolated [3]. The layer-by-layer approach of LPBF allows the optimization of the MLS design regarding weight and functionality as location and part-specific tailoring of mechanical properties, such as strength, stiffness, fatigue life, or energy absorption.

Despite its capabilities, LPBF can introduce various defects during the manufacturing process. The defects in LPBF of metals can be attributed to various factors related to the process, alloy composition, powder properties, process parameters, and environmental conditions in the chamber. Destructive testing methods like tensile testing mainly shed light on a material's mechanical properties, including its elasticity, strength, and ductility. Destructive testing techniques do not directly evaluate or discover internal faults, but they possibly indicate the existence of such problems if the measured strength differs significantly from the expectations following the test. Rather, they could spur more research to ascertain the reason for the departure from anticipated outcomes, which might involve looking into internal defects. Conversely, non-destructive testing methods are designed expressly to identify and examine internal imperfections in materials without causing any changes, thereby offering more precise information on the material's integrity.

Non-destructive testing consists of techniques to assess the structural soundness of materials, detect surface or internal defects, or evaluate metallurgical conditions without causing any damage to the material or compromising its suitability for use [4]. Non-destructive testing encompasses various methods designed to identify and assess anomalies to prevent the worsening of a product's condition and facilitate potential rectification. A key benefit of non-destructive testing is its applicability throughout all product life stages, including during its operational phase. This enables precise determination of the defect location, properties such as dimensions; propagation rate, and the severity of the possible imperfection [5]. A diverse range of non-destructive techniques or methods are available [6], suitable for application on metals, plastics, ceramics, and composites, e.g., visual inspection [7], microscopy [8], radiography [9], dye penetration [10], ultrasonic [11], magnetic particle [12], eddy current [13], and acoustic emission [14].

The impulse excitation technique (IET) allows the identification of the non-destructive material attributes. Using a short mechanical or acoustic impact, the test object and its natural frequencies are excited. Those frequencies are collected by a sensitive

microphone. The mass of the item and its stiffness, which are defined by its size, shape, and material's modulus of elasticity, define the natural frequency [15]. This work investigates how IET could be used to compare the stiffness of MLS and to evaluate macro-scale imperfections in lattice and bulk parts by using the natural frequency differences as an efficient NDI method.

2. Material and methods

2.1 Sample production

A ProX® DMP320 3D printer from 3D Systems (Belgium) was used as an LPBF setup, as shown in Fig. 1, to produce 9 MLS in the aluminium A205 alloy. A205 is a high-strength Al–Cu–Mg–Ag–Ti–B alloy which was used in powder form with a particle size ranging from 20 μm (D_{10}) to 63 μm (D_{90}) [16]. The layer thickness for all samples was 30 μm and the feed was single-sided. All job files were prepared using 3D Systems 3DXpert software.

Fig 1. 3D Systems ProX® DMP 320.

In total, nine samples were produced, all with different features. The outer dimensions of all samples were 20×20×50 mm³. Two samples were bulk and the rest were designed as lattice structures with different properties. Three of the lattice structures were based on strut-based diamond unit cell and four were based on triply periodic minimal surface (TPMS) gyroid unit cell. Two of the four gyroid lattices contain two flat surfaces (bulk regions) with a thickness of 0.25 mm on the lower and upper faces. Unit cell dimensions and strut thicknesses were the same for all lattices, respectively being 2×2×2 mm³ and 0.4 mm. All samples are listed in Table 1.

The average masses of the gyroid with bulk panels, bulk, diamond, and gyroid sample groups were 23.4 ± 0.03 g, 57 ± 0.01 g, 10.3 ± 0.02 g, and 22.2 ± 0.03 g, respectively. The masses of the samples associated with the respective groups can be regarded as approximately

equivalent. Therefore, the detection of induced defects using the IET has a significant importance. The samples were removed from the base plate with a wire electrical discharge machining (W-EDM) machine. Additional height was incorporated into the lower part of the structures to account for the material removal during W-EDM.

Table 1. Sample specifications for non-defected samples and samples with an induced defect zone.

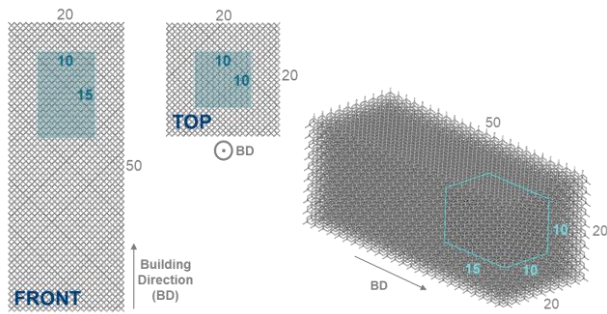| # of Sample	Geometry of the Sample
1	Gyroid with panels with defect zone
2	Bulk with defect zone
3	Bulk
4	Diamond with bulk parameters
5	Gyroid with defect zone
6	Gyroid with panels
7	Diamond with defect zone
8	Diamond
9	Gyroid

The average masses of the gyroid with bulk panels, bulk, diamond, and gyroid sample groups were 23.4 ± 0.03 g, 57 ± 0.01 g, 10.3 ± 0.02 g, and 22.2 ± 0.03 g, respectively. The masses of the samples associated with the respective groups can be regarded as approximately equivalent. Therefore, the detection of induced defects using the IET has a significant importance. The samples were removed from the base plate with a wire electrical discharge machining (W-EDM) machine. Additional height was incorporated into the lower part of the structures to account for the material removal during W-EDM.

The concept of virtual volume (VV) was used to assign suboptimal LPBF processing parameters to small volumes such that engineered defects could be introduced in the samples. The selectively placed VV is illustrated in Fig. 2.

For the VV region, the process parameters are diverted from the identified optimum: laser power is halved and speed is increased by 25% compared to bulk printing parameters. It is expected that these parameters induce defects. They are further referred to as suboptimal parameters. In order to be detected by IET, all VVs were positioned at the same place in all samples. The bounding volume of the VVs is 10×10×15 mm³.

The process parameters identified as optimal for bulk samples, namely a laser power of 263 W and a scanning speed of 1250 mm/s, were applied to both gyroid structures (with and without panels) and bulk samples. A contour-infill scan strategy was applied with a 100 μm hatch spacing, 50 μm contour offset, and a bidirectional infill with a 90° rotation of the infill vectors between the layers. Process parameters optimized for thin strut-based lattice structures were used for the diamond unit

cell samples. A multi-contour scan strategy was applied using an 80 μm offset, laser power of 130 W, and scanning speed of 900 mm/s. In addition, optimal lattice parameters leading to a high material density include skywriting off [16]. The VV and one whole diamond lattice structure were printed using suboptimal LPBF parameters. The bulk specimen with a VV zone is shown in Fig. 3.

Fig 2. MLS sample geometry with the indication of VV. (All dimensions are in mm.)

For the VV region, the process parameters are diverted from the identified optimum: laser power is halved and speed is increased by 25% compared to bulk printing parameters. It is expected that these parameters induce defects. They are further referred to as suboptimal parameters. In order to be detected by IET, all VVs were positioned at the same place in all samples. The bounding volume of the VVs is 10×10×15 mm³.

The process parameters identified as optimal for bulk samples, namely a laser power of 263 W and a scanning speed of 1250 mm/s, were applied to both gyroid structures (with and without panels) and bulk samples. A contour-infill scan strategy was applied with a 100 μm hatch spacing, 50 μm contour offset, and a bidirectional infill with a 90° rotation of the infill vectors between the layers. Process parameters optimized for thin strut-based lattice structures were used for the diamond unit cell samples. A multi-contour scan strategy was applied using an 80 μm offset, laser power of 130 W, and scanning speed of 900 mm/s. In addition, optimal lattice parameters leading to a high material density include skywriting off [16]. The VV and one whole diamond lattice structure were printed using suboptimal LPBF parameters. The bulk specimen with a VV zone is shown in Fig. 3.

2.2 Melt pool monitoring

The DMP melt pool monitoring system was integrated into the ProX® DMP 320 to monitor each layer's light intensity during printing. Light intensity is related to the energy of the melt pool. More specifically, two off-axis photodiodes were used to capture meltpool irradiation as explained extensively in [18]. If the data is presented in its original logging format, it can be challenging for a user to identify significant patterns. Instead, to display the data, the temporal aspect is eliminated, and the recorded intensity is depicted as a false color point at the position of the laser spot

corresponding to the time of the intensity measurement. Fig. 4 shows false-color plots of the melt pool intensity data of two layers with and without VV. High-intensity and low-intensity zones are given as yellow and blue colors, respectively. The figure illustrates that areas scanned with suboptimal parameters are displayed in blue due to low energy intensity as for suboptimal process parameters the power is reduced and speed is increased, while other parts are depicted in yellow because they were scanned with the higher energy intensity of optimal process parameters.
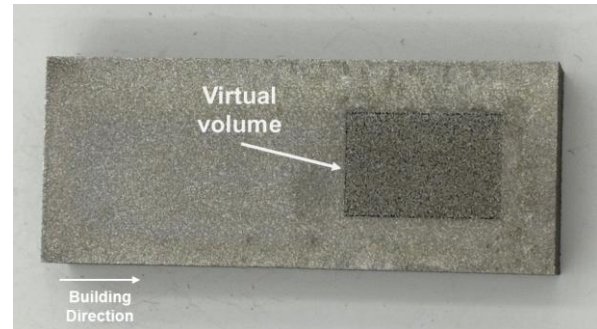
Fig 3. Bulk specimen with visible VV zone after EDM.

2.3 Non-destructive testing

All non-destructive tests were performed with a GrindoSonic MK7 IET system with a hammer to trigger the sample and a microphone to capture the resonance frequencies. For insulation, a piece of foam was placed under the specimens for each test. For each specific sample test, different bandpass filters were chosen to capture the natural frequencies accurately. All tests were performed in accordance with the ASTM E1876 Standard Test Method for Dynamic Young's Modulus, Shear Modulus, and Poisson's Ratio by Impulse Excitation of Vibration standard. Fig. 5 shows the IET setup, the microphone position and the excitation point.
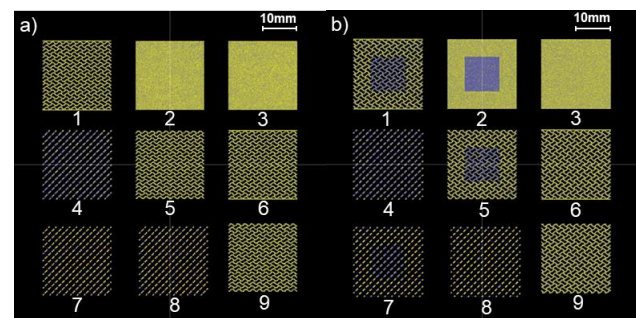

Fig 4. False-color plots (top view) of a layer without VV (a) and a layer with VV (b). (blue= low intensity; yellow= high intensity).

2.4 Microstructural investigation

In order to verify the internal defects, a cross-section of all specimens parallel to the building direction was performed. Samples were embedded in Technovit 4004

resin, ground up to SiC grain size 4000, polished up to a diamond polishing suspension of 1 micron, and finished with a colloidal Silica Oxide Polishing Suspension (OPS) [19]. The cross-sections were further investigated with a Keyence VHX-6000 3D optical stereomicroscope.
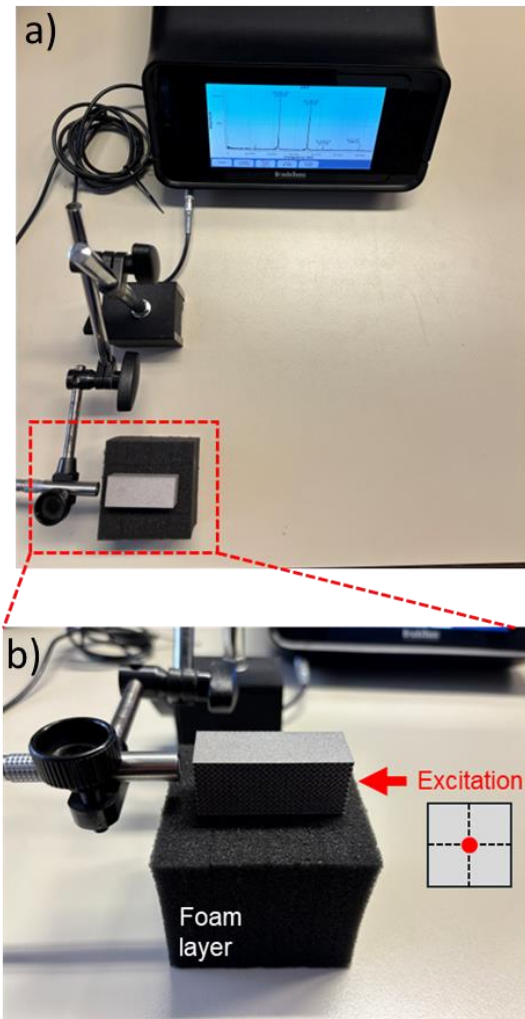

Fig 5. Natural frequency measurement of a lattice sample with IET. a) IET setup b) microphone, foam layer, and excitation point.

3. Results and discussion

## 3.1 Microstructural analysis

Due to the change of process parameters in the VV region to suboptimal parameters, a higher amount of internal defects occurred in these regions. The main reason for these porosities is the lack of fusion. These porosities inside the struts, formed in the defected zone are clear in Fig. 6 which shows a polished cross-section parallel to the building direction. Compared to the area scanned with standard lattice parameters, it contains significantly more porosities.

With a similar approach, porosities (white zones) formed due to lack of fusion and negatively affecting the mechanical properties of the sample were observed not only in lattice specimens but also in bulk samples. These defects are indicated in Fig. 7.
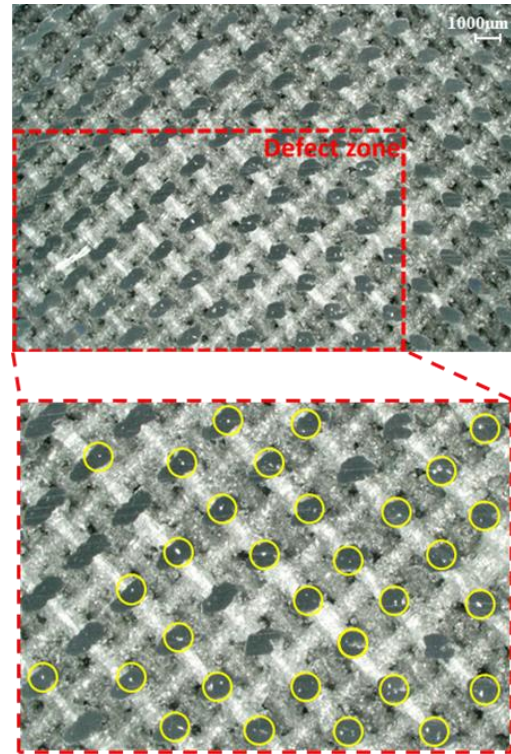
Fig 6. Optical microscope images of the porosities (white zones) inside the struts of a lattice specimen due to lack of fusion.
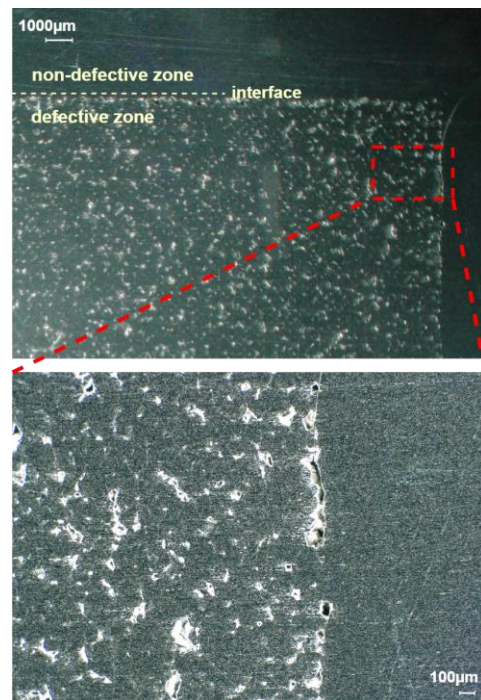
Fig 7. Optical microscope image of a bulk sample showing the difference in porosity between suboptimal and optimal process parameters in respectively the VV zone and the rest of the sample.

3.2 IET measurements

The results of the compressive mode exciting of all nine samples are plotted in Fig. 8.

Infinite Science | Publishing
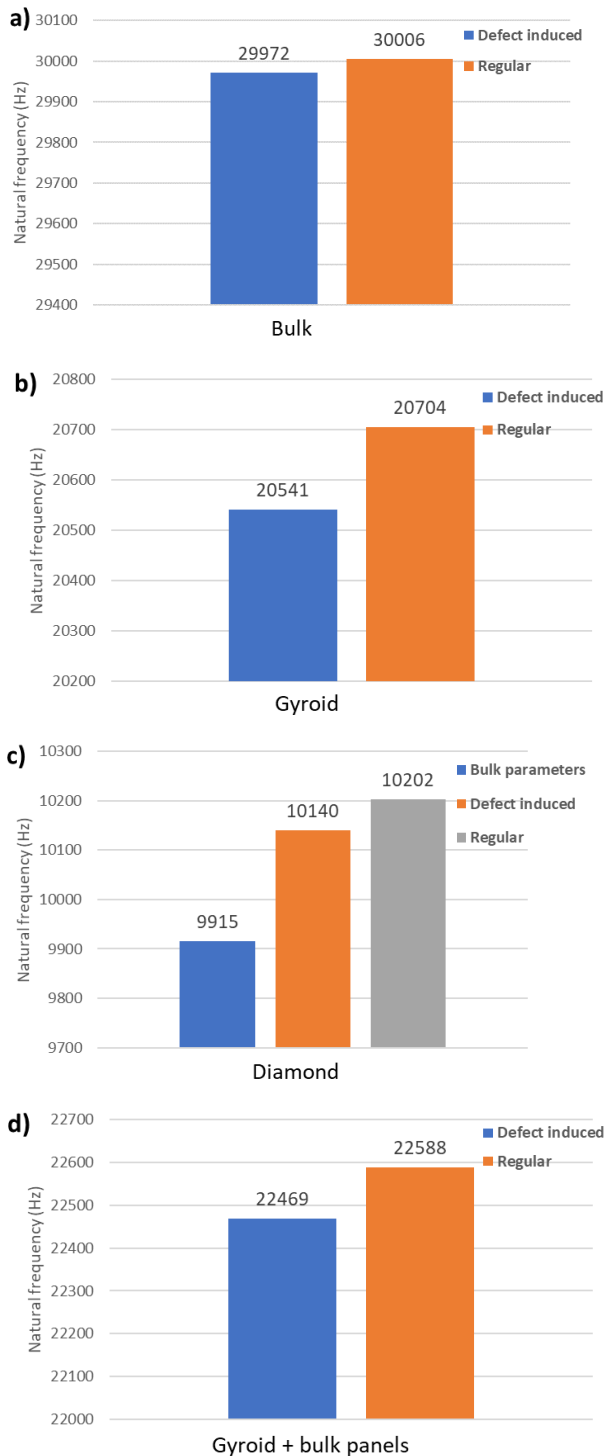
Fig 8. Average natural frequencies were collected with IET for nine different samples.

Compared to the diamond lattice set the IET test results of samples with identical geometries but with and without a VV show that the resonant frequencies are different. In this way, the detection of selectively placed VVs or the differences in mechanical properties of prints made with partially different parameters can be understood in a non-destructive way. Looking at the general pattern, samples with defects have lower resonant frequencies, while samples without defects have higher frequencies. Each test was repeated three times to quantify the deviations in the test results. Fig.

9 summarizes the standard deviations of the natural frequencies for each sample. The standard deviations are very small, providing an indication the effect of false positives and false negatives is very limited.

Samples with induced defects have lower resonance frequencies because of a stiffness decrease, as can be understood from the relationship between stiffness and natural frequency in Equation (1). Since the mass difference between geometrically identical samples is negligible, the natural frequency is directly proportional to the axial stiffness. Additionally, the stiffness decrease may also cause a fatigue life reduction under dynamic loads.

$$w_{natural} = \sqrt{k_{axial}/m} \qquad (1)$$
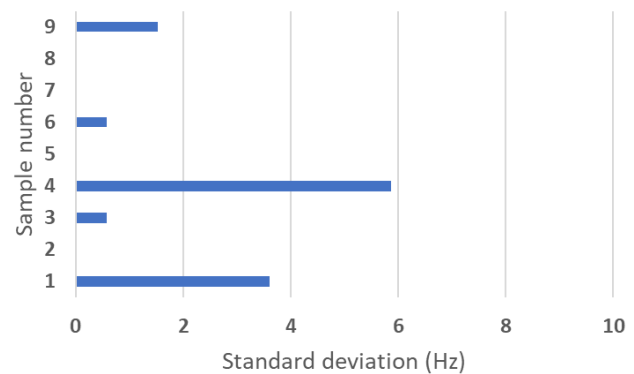
Fig 9. Standard deviations of the three measurements for each sample.

4. Conclusions

This work explores resonant frequency differences by using IET, a non-destructive test method, instead of using destructive methods in detecting selectively placed defects in strut-based diamond, TPMS gyroid lattice, and bulk samples produced with LPBF. As a result of the tests, it is shown that defective samples have lower resonant frequencies compared to non-defective ones despite only a negligible difference in mass. Hence defective samples could be detected by taking advantage of this difference. Additionally, the acquired false-color plots from in-situ melt pool monitoring data can be correlated well with the virtual volumes, hence the zones in which lack of fusion porosities are induced via suboptimal process parameters and are detected via non-destructive IET testing.

Author's statement

References

1. Cutolo, A., Beevers, E., & Van Hooreweder, B. (2023). A design strategy to enhance the mechanical response of diamond-based lattice structures produced by laser powder bed fusion. Materials Science and Engineering: A, 876, 145120.
2. Babaee, S., Jahromi, B. H., Ajdari, A., Nayeb-Hashemi, H., & Vaziri, A. (2012). Mechanical properties of open-cell rhombic dodecahedron cellular structures. Acta Materialia, 60(6-7), 2873-2885.
3. Roberts, A. P., & Garboczi, E. J. (2001). Elastic moduli of model random three-dimensional closed-cell cellular solids. Acta materialia, 49(2), 189-197.
4. Cawley; Non-destructive testing—current capabilities and future directions; Journal of Materials: Design and Applications; October 1, 2001 vol. 215 (213-223).
5. Gupta, M., Khan, M. A., Butola, R., & Singari, R. M. (2022). Advances in applications of Non-Destructive Testing (NDT): A review. Advances in Materials and Processing Technologies, 8(2), 2286-2307.
6. Dwivedi, S. K., Vishwakarma, M., & Soni, A. (2018). Advances and researches on non destructive testing: A review. Materials Today: Proceedings, 5(2), 3690-3698.
7. Bortak, Tom N. *Guide to Protective Coatings Inspection and Maintenance*. US Department of the Interior, Bureau of Reclamation, 2002.
8. Aryan, Pouria, Santhakumar Sampath, and Hoon Sohn. "An overview of non-destructive testing methods for integrated circuit packaging inspection." Sensors 18.7 (2018): 1981.
9. Strobl, M., et al. "Advances in neutron radiography and tomography." Journal of Physics D: Applied Physics 42.24 (2009): 243001.
10. Yoshikawa, Takako, et al. "Environmental SEM and dye penetration observation on resin-tooth interface using different light curing method." Dental Materials Journal 35.1 (2016): 89-96.
11. Su, Lei, et al. "Defect inspection of flip chip solder bumps using an ultrasonic transducer." Sensors 13.12 (2013): 16281-16291.
12. Bowler, John R., and Nicola Bowler. "Evaluation of the magnetic field near a crack with application to magnetic particle inspection." Journal of Physics D: applied physics 35.18 (2002): 2237.
13. Zhou, Xiuyun, et al. "Research on defects inspection of solder balls based on eddy current pulsed thermography." Sensors 15.10 (2015): 25882-25897.
14. Petit, Johann, Guillaume Montay, and Manuel François. "Strain localization in mild (low carbon) steel observed by acoustic emission-ESPI coupling during tensile test." Experimental Mechanics 58 (2018): 743-758.
15. A. Nabhan et al., (2015) EGTRIB Journal of The Egyptian Society of Tribology. 12, 15–29
16. "A205 Data Sheet A20X 2020v5." A20X, Sept. 2020, https://a20x.com/wp-content/uploads/2020/09/A205_Data-Sheet_A20X_2020v5.pdf. Accessed May 2024.
17. Beevers, E., & Van Hooreweder, B. (2023, March). Effect of unit cell topology on the fatigue performance of aluminium lattice structures produced by L-PBF. In ECSSMET23, European Conference on Spacecraft Structures, Materials and Environmental Testing, Date: 2023/03/28-2023/03/30, Location: Centre de Congrès Pierre Baudis, Toulouse, France.
18. Coeck, S., Bisht, M., Plas, J., & Verbist, F. (2019). Prediction of lack of fusion porosity in selective laser melting based on melt pool monitoring data. Additive Manufacturing, 25, 347-356.
19. Beevers, E., Cutolo, A., Mertens, F., & Van Hooreweder, B. (2023). Unravelling the relation between Laser Powder Bed Fusion processing parameters and the mechanical behaviour of as built lattices in a novel Al–Cu–Mg–Ag–Ti–B alloy. Journal of Materials Processing Technology, 315, 117915.